Physics and Imaging in Radiation Oncology 5 (2018) 5–8

Contents lists available at ScienceDirect

Physics and Imaging in Radiation Oncology

journal homepage: www.elsevier.com/locate/phro

Short Communication

Uncertainty evaluation of image-based tumour control probability models in radiotherapy of prostate cancer using a visual analytic tool

Oscar Casares-Magaz[a,1,*], Renata G. Raidou[b,1], Jarle Rørvik[d,e], Anna Vilanova[c], Ludvig P. Muren[a,2]

[a] Department of Medical Physics, Aarhus University Hospital/Aarhus University, Aarhus, Denmark
[b] Institute of Computer Graphics and Algorithms, Vienna University of Technology, Austria
[c] Delft University of Technology, The Netherlands
[d] Department of Clinical Medicine, University of Bergen, Bergen, Norway
[e] Department of Radiology, Haukeland University Hospital, Bergen, Norway

ARTICLE INFO

Keywords:
Tumour control probability
Visualization tool
Uncertainties
Apparent diffusion coefficient (ADC) maps
Prostate cancer

ABSTRACT

Functional imaging techniques provide radiobiological information that can be included into tumour control probability (TCP) models to enable individualized outcome predictions in radiotherapy. However, functional imaging and the derived radiobiological information are influenced by uncertainties, translating into variations in individual TCP predictions. In this study we applied a previously developed analytical tool to quantify dose and TCP uncertainty bands when initial cell density is estimated from MRI-based apparent diffusion coefficient maps of eleven patients. TCP uncertainty bands of 16% were observed at patient level, while dose variations bands up to 8 Gy were found at voxel level for an *iso*-TCP approach.

1. Introduction

Tumour control probability (TCP) models are developed to predict radiotherapy (RT) outcomes, both across populations and on a patient-specific level [1,2]. Initial TCP modelling studies assumed spatially uniform distributions of radiobiological characteristics, both within and between patients [3]. There is currently considerable interest in integrating and adapting RT according to biological information acquired during all stages of the treatment process [4]. In recent TCP studies, patient-specific tumour information including features related to inter- and intra-tumour heterogeneities have been incorporated into the models, while also considering different dose distributions patterns within the tumour for maximum tumour control [5]. Some of these models exploit the benefit of functional imaging that non-invasively provides information on tumour characteristics [6]. However, this information may be influenced by inherent inaccuracies in the image acquisition process, which in turn leads to uncertainties in the TCP model.

Uncertainty in the TCP models, as well as the underlying tumour information may be difficult to explore and analyse. Methods from the field of Visual Analytics (VA) – a discipline that combines visualization with semi-automatic methods of data analysis [7] – could be used to explore and analyse the TCP models. The particular application of VA to TCP models may facilitate the inclusion of uncertainties associated with biological information and the visualization of patient-specific TCP uncertainty bands.

The aim of the present work was therefore to quantify uncertainty bands by using a previously developed VA tool [8], built to include Apparent Diffusion Coefficient (ADC)-induced uncertainties in the TCP calculation, when ADC maps were used to calculate the initial number of clonogens [9]. The study was based on ADC maps of patients with prostate cancer and explored the uncertainties associated with two different approaches to relate ADC values to cell densities.

2. Materials and methods

2.1. Patient information

Magnetic Resonance Imaging (MRI)-based ADC maps derived from diffusion weighted imaging (DWI) together with index-volume contours of eleven prostate cancer patients were included in this study. Image data sets were acquired using an integrated endorectal and pelvic

* Corresponding author at: Aarhus University Hospital/Aarhus University, Department of Medical Physics, Nørrebrogade 44, Building 5, 8200 Aarhus, Denmark.
E-mail address: oscar.casares@oncology.au.dk (O. Casares-Magaz).

[1] Both authors contributed equally to this work.

[2] Dr. Ludvig Muren, a co-author of this paper, is Editor-in-Chief of Physics & Imaging in Radiation Oncology. A member of the Editorial Board managed the editorial process for this manuscript independently from Dr. Muren and the manuscript was subject to the Journal's usual peer-review process.

https://doi.org/10.1016/j.phro.2017.12.003
Received 7 September 2017; Received in revised form 15 December 2017; Accepted 21 December 2017

Table 1
Dose and TCP bands, and voxel dose variability for all the patients, assuming the ADC uncertainties inside the index lesion at the two different levels of total TCP, 0.7 and 0.9 ($TCP_{0.7}$ and $TCP_{0.9}$ respectively), and for the two cell density approaches.

Patient (N)	Index Volume (%)	Voxel Dose Variability (Gy)				Dose Uncertainty (Gy, mean ± SD)			
		Linear $TCP_{0.7}$	Linear $TCP_{0.9}$	Sigmoid $TCP_{0.7}$	Sigmoid $TCP_{0.9}$	Linear $TCP_{0.7}$	Linear $TCP_{0.9}$	Sigmoid $TCP_{0.7}$	Sigmoid $TCP_{0.9}$
1	5	0.94	0.96	4.23	4.32	1.1 ± 0.3	1.00 ± 0.0	1.6 ± 0.7	1.1 ± 0.3
2	3	1.28	1.30	1.34	1.47				
3	8	1.05	1.07	2.57	2.60	TCP Uncertainty (%, mean ± SD)			
4	6	1.00	1.05	2.56	2.57	Linear $TCP_{0.7}$	Linear $TCP_{0.9}$	Sigmoid $TCP_{0.7}$	Sigmoid $TCP_{0.9}$
5	11	1.10	1.14	1.92	1.99				
6	5	0.88	0.93	0.95	0.97	3.2 ± 0.4	2.2 ± 0.4	6.5 ± 4.7	4.7 ± 3.4
7	17	1.13	1.17	2.58	2.62				
8	8	0.93	0.95	3.56	3.63	Mean Dose for Iso-TCP (Gy, mean ± SD)			
9	20	0.92	0.96	0.74	0.57	Linear $TCP_{0.7}$	Linear $TCP_{0.9}$	Sigmoid $TCP_{0.7}$	Sigmoid $TCP_{0.9}$
10	1	1.63	1.74	4.50	4.68				
11	2	1.06	1.05	1.32	1.25	109.9±7.7	117.9±7.9	92.4±6.5	100.1±6.5

phased-array coil in a 1.5 T whole body MRI unit Siemens Avanto (Siemens Medical Systems, Erlangen, Germany). Further information on image acquisition, post-processing and patient characteristics were described by Reisæter et al. [10].

2.2. Visual analysis tool

A VA tool was developed [8] to evaluate the propagation of uncertainties into TCP calculations, caused by cell density estimations from MRI-based ADC maps in prostate cancer patients [9]. In brief, the proposed VA framework incorporated the following four main components: (1) It supported quantification and exploration of ADC-induced uncertainty (cell density uncertainties within the index lesion derived from ADC maps) and its propagation to TCP modelling; (2) it facilitated exploration and analysis of the sensitivity of TCP models to different assumptions and parameter variations; (3) it enabled identification and exploration of inter-patient response variability within cohorts; (4) it allowed, given a targeted treatment outcome, to identify the treatment strategies or parameters that would achieve it.

2.3. Cell density, ADC uncertainties and TCP computations

The cell density at each voxel within the index lesion was calculated using two different approaches: (1) A linear relation between ADC and cell density [11]; (2) an inverse sigmoid relation between ADC and cell densities, with cell densities in the range of 10^5–10^7 cell/cm^3. Voxels outside the index lesion were considered to have a constant cell density of 10^5 cell/cm^3 for both cases; further details about the two different approaches to derive cell densities have been described elsewhere [9].

ADC map uncertainties were included in the calculations of voxel cell densities based on the results of a multicentre study previously performed across three different clinical platforms, where ADC maps from a phantom and a volunteer (http://drtherapat.eu/deliverables/reports/) were derived by using the same image sequences. The ADC value at each voxel was then modelled as a Gaussian distribution, assuming a standard deviation (σ) of 3% of the unknown real value. From this, the quantitative real ADC value at each voxel position was estimated by an analytical approximation of the probability that the real value occurred, given the measured ADC value. The uncertainties on ADC values for the experimental data were also considered to compute the linear relation between volumetric cell density and measured ADC values [8].

TCP modelling was based on Linear-Quadratic (LQ) curves, combined with a Poisson dose–response model. The LQ model parameters were set as: $\alpha = 0.18\,Gy^{-1}$ and $\alpha/\beta = 1.93\,Gy$, and considering an intra-tumour normal distribution of both α and β of 15% [12].

2.4. Evaluation of the tool

The eleven patients were loaded into the visualization tool frame, assuming the aforementioned radiobiological parameters, the two different approaches for the relation between cell density and ADC values, and the voxel-wise intrinsic uncertainty bands for the ADC maps.

TCP bands for each patient derived from the uncertainties in the cell density were calculated assuming a prescribed dose of 95 Gy in 2.7 Gy/fraction to the index lesion, while the rest of prostate received concomitantly 77 Gy in 2.2 Gy/fraction, mimicking an integrated boost treatment [13]. The overall patient TCP and dose uncertainty bands were evaluated at two different levels of the mean TCP: 0.7 ($TCP_{0.7}$) and 0.9 ($TCP_{0.9}$). TCP levels and dose uncertainties bands were compared using paired *t*-test.

Additionally, assuming voxel-wise *iso*-TCP distributions across the whole prostatic volumes for the overall patient $TCP_{0.7}$ and $TCP_{0.9}$ levels, mean dose per voxel and the associated dose uncertainty bands were also calculated.

3. Results

The ratio between the index volume and prostate volume ranged from 1% to 20% across the eleven patients. Across the population, the ADC values inside the index lesion (mean ± SD: 1.07 ± 0.17·10^3 mm^2/s) were lower than outside the index (1.22 ± 0.16·10^3 mm^2/s), indicating higher cell density values inside the index lesion (Table 1).

The visualization tool allowed quantification of TCP and dose uncertainty bands at each subject and at different levels of the overall mean TCP. For $TCP_{0.7}$, the individual TCP bands ranged between 3% and 4% across the patients for the linear approach, and between 1% and 16% for the sigmoid approach. At $TCP_{0.9}$, the TCP uncertainty bands ranged from 1% to 3% for the linear approach, and from 1% to 11% using the sigmoid approach.

Mean doses at the index volume needed to achieve the overall patient $TCP_{0.7}$ and $TCP_{0.9}$ levels (*iso*-TCP for all voxels) were 110 Gy and 118 Gy for the linear approach; and 92 Gy and 100 Gy for the sigmoid approach, reflecting the lower cell density values resulting from the

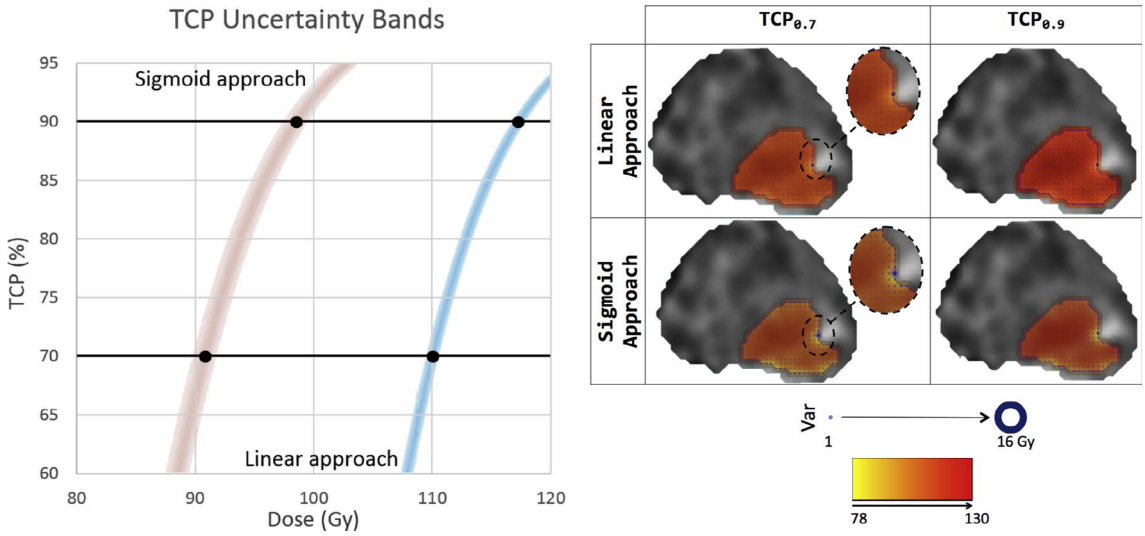

Fig. 1. Left Panel: Uncertainty bands for one the patients and for the two different approaches to relate cell density and ADC values, assuming an *iso*-TCP for all the voxels inside the prostate. Right Panel: Index and prostate contours over the ADC maps for one plane at the central part of the prostate for the same patient; showing mean dose and dose variability (blue circles) at the voxel level for the two density approaches and for the two TCP levels. (For interpretation of the references to colour in this figure legend, the reader is referred to the web version of this article.)

latter (Table 1).

Dose variability bands were similar for all patients and for the two TCP levels (0.7 and 0.9), ranging between 1 Gy and 2 Gy for the linear approach, and between 1 Gy and 3 Gy for the sigmoid approach. TCP variability bands were slightly higher at the $TCP_{0.7}$ level compared to those at $TCP_{0.9}$ level (mean ± SD, 1.1 ± 0.3 Gy vs. 1.0 ± 0.0 Gy linear approach, *t*-test p-value < .05; 1.6 ± 0.7 Gy vs. 1.1 ± 0.3 Gy sigmoid approach, *t*-test p-value < .05). The TCP bands followed the same trend, and wider ranges were observed for the sigmoid compared to the linear approach (mean ± SD, 3.2 ± 0.4% vs. 2.2 ± 0.4% linear approach, 6.5 ± 4.7% vs. 4.7 ± 3.4% sigmoid approach). At voxel-level, the mean dose variability was similar at the two dose levels (1.1 Gy and 2.4 Gy for the linear and sigmoid approaches respectively, Table 1, Fig. 1).

4. Discussion

In the present study we have evaluated a TCP visualization tool previously developed to quantify uncertainties in dose and TCP when functional imaging information was used to estimate radiobiological parameters. We observed patient specific TCP variations (up to 16%) and voxel specific dose variations (up to 8 Gy) when uncertainties were included in the estimation of the radiobiological information in a data set of prostate cancer patients. This study included the evaluation of two different approaches (a linear and a sigmoid model) to calculate cell density from ADC maps. The linear model represented the experimental relation observed between ADC values and cell density [11] resulting in denser tissues, while the sigmoid model included conventional values for prostate tissue density, used in previous TCP models.

To the best of our knowledge this is the first study showing the suitability of a VA tool [8] to evaluate individual image-based TCP bands after RT in the presence of uncertainties. More specifically, this study exemplifies propagation of imaging uncertainty into image-based TCP models for RT of prostate cancer, by the inclusion of three tumour parameters: the index volume, the prostate volume and the clonogenic cell density extracted from ADC maps. Although patient-specific ADC time variations are negligible [14], ADC map acquisition has poor reproducibility across centres and scanners, having a limited spatial resolution and non-straight forward translation into specific radiobiological parameters [15]. Therefore, the latter limitations should be considered in future perspectives, or if further tumour information is included in the models. Additionally, MRI acquisitions require extra time and resources, while at the same time provide patient-specific radiobiological information. Tools like the one presented here might be suitable for incorporation into clinical routine, providing important information for treatment selection or pre- and post-treatment evaluation.

In the present study, tumour size and cell density were incorporated into the model to estimate patient's TCPs. Also other tumour parameters, such as radio-sensitivity, oxygenation or tumour proliferation, might play a more important role in the overall treatment response. These other radiobiological features may also be extracted using functional imaging [16], and generalization to a more complete biological description may lead to a more individualized and accurate tumour control probability estimation. Several studies have aimed to predict prostate tumour presence from multi-parametric MRI [17,18], which enabled radiobiological optimization of dose distributions based on tumour presence probability and functional imaging uncertainties [19]. Additionally associations between imaging patterns and histopathological features were used to score tumour aggressiveness and/or activity [20], and other recent studies identified MRI-based predictive biomarkers of radiation response, being mostly associated with tumour hypoxia [21,22]. Therefore, more sophisticated numerical methods, e.g. support vector machine or vector recognition, are needed to increase ability to determine tumour features [5,23,24]. Besides, each imaging modality that can be incorporated in the model carry uncertainties that need to be explored and their effect on the final TCP outcome needs to be analyzed.

The inclusion of uncertainties in TCP calculations together with patient-specific tumour biology features may allow evaluation of RT plan suitability and be relevant for the treatment decision making processes. Besides, this tool can also be part of biological-targeted dose optimization process, where not only tumour information is used to estimate the ideal dose distribution, but also to redistribute the dose in order to minimize uncertainties. Besides, this tool has the potential of performing patient clustering, where similar patients can be recognized based on their tumour characteristics.

In conclusion, by using a VA tool this study has estimated dose and TCP bands, as well as voxel dose variability owing to ADC uncertainties for prostate cancer patients, when ADC maps are used to estimate cell densities inside index lesions. Further improvements in functional imaging to increase accuracy in radiobiological parameter estimations

may increase the need for such tools to predict individual tumour responses before RT, enabling more appropriate dose prescriptions or biologically guided dose painting.

Conflicts of interest

None.

References

[1] Kok D, Gill S, Bressel M, Byrne K, Kron T, Fox C, et al. Late toxicity and biochemical control in 554 prostate cancer patients treated with and without dose escalated image guided radiotherapy. Radiother Oncol 2013;107:140–6.

[2] Lindblom E, Dasu A, Lax I, Toma-Dasu I. Survival and tumour control probability in tumours with heterogeneous oxygenations: a comparison between the linear-quadratic and the universal survival curve models for high doses. Acta Oncol 2014;53:1–6.

[3] Webb S, Nahum AE. A model for calculating tumour control probability in radiotherapy including the effects of inhomogeneous distributions of dose and clonogenic cell density. Phys Med Biol 1993;38:653–66.

[4] Grau C, Overgaard J, Høyer M, Tanderup K, Lindegaard JC, Muren LP. Biology-guided adaptive radiotherapy (BiGART) is progressing towards clinical reality. Acta Oncol 2015;54:1245–50.

[5] Thorwarth D. Biologically adapted radiation therapy. Z Med Phys 2017.

[6] Dirscherl T, Rickhey M, Bogner L. Feasibility of TCP-based dose painting by numbers applied to a prostate case with (18)F-choline PET imaging. Z Med Phys 2012;22:48–57.

[7] Keim DA, Mansmann F, Schneidewind J, Thomas J, Ziegler H. Visual analytics: scope and challenges. Vis Data Min, Berlin, Heidelberg: Springer, Berlin Heidelberg 2008:76–90.

[8] Raidou RG, Casares-Magaz O, Muren LP, van der Heide UA, Rørvik J, Breeuwer M, et al. Visual analysis of tumor control models for prediction of radiotherapy response. Comput Graph Forum 2016;35:231–41.

[9] Casares-Magaz O, van der Heide UA, Rørvik J, Steenbergen P, Muren LP. A tumour control probability model for radiotherapy of prostate cancer using magnetic resonance imaging-based apparent diffusion coefficient maps. Radiother Oncol 2016;119:111–6.

[10] Reisæter LA, Fütterer JJ, Halvorsen OJ, Nygård Y, Biermann M, Andersen E, et al. 1.5-T multiparametric MRI using PI-RADS: a region by region analysis to localize the index-tumor of prostate cancer in patients undergoing prostatectomy. Acta Radiol 2014;56:500–11.

[11] Gibbs P, Liney GP, Pickles MD, Zelhof B, Rodrigues G, Turnbull LW. Correlation of ADC and T2 measurements with cell density in prostate cancer at 3.0 Tesla. Invest Radiol 2009;44:572–6.

[12] Brenner DJ, Hlatky LR, Hahnfeldt PJ, Hall EJ, Sachs RK. A convenient extension of the linear-quadratic model to include redistribution and reoxygenation. Int J Radiat Oncol Biol Phys 1995;32:379–90.

[13] Lips IM, van der Heide UA, Haustermans K, van Lin ENJT, Pos F, Franken SPG, et al. Single blind randomized phase III trial to investigate the benefit of a focal lesion ablative microboost in prostate cancer (FLAME-trial): study protocol for a randomized controlled trial. Trials 2011;12:255.

[14] Morgan VA, Riches SF, Thomas K, Vanas N, Parker C, Giles S, et al. Diffusion-weighted magnetic resonance imaging for monitoring prostate cancer progression in patients managed by active surveillance. Br J Radiol 2011;84:31–7.

[15] Vogel WV, Lam MGEH, Pameijer FA, van der Heide UA, van de Kamer JB, Philippens ME, et al. Functional imaging in radiotherapy in the Netherlands: availability and impact on clinical practice. Clin Oncol 2016;28:e206–15.

[16] Han SH, Ackerstaff E, Stoyanova R, Carlin S, Huang W, Koutcher JA, et al. Gaussian mixture model-based classification of dynamic contrast enhanced MRI data for identifying diverse tumor microenvironments: preliminary results. NMR Biomed 2013;26:519–32.

[17] Weinreb JC, Barentsz JO, Choyke PL, Cornud F, Haider MA, Macura KJ, et al. PI-RADS prostate imaging – reporting and data system: 2015, version 2. Eur Urol 2016;69:16–40.

[18] Litjens GJS, Hambrock T, Hulsbergen–van de Kaa C, Barentsz JO, Huisman HJ. Interpatient variation in normal peripheral zone apparent diffusion coefficient: effect on the prediction of prostate cancer aggressiveness. Radiology 2012;265:260–6.

[19] Alber M, Thorwarth D. Multi-modality functional image guided dose escalation in the presence of uncertainties. Radiother Oncol 2014;111:354–9.

[20] Ghobadi G, de Jong J, Hollmann BG, van Triest B, van der Poel HG, Vens C, et al. Histopathology-derived modeling of prostate cancer tumor control probability: implications for the dose to the tumor and the gland. Radiother Oncol 2016;119:97–103.

[21] Hallac RR, Zhou H, Pidikiti R, Song K, Stojadinovic S, Zhao D, et al. Correlations of noninvasive BOLD and TOLD MRI with pO2 and relevance to tumor radiation response. Magn Reson Med 2014;71:1863–73.

[22] Zhao D, Pacheco-Torres J, Hallac RR, White D, Peschke P, Cerdán S, et al. Dynamic oxygen challenge evaluated by NMR T1 and $T2^*$–insights into tumor oxygenation. NMR Biomed 2015;28:937–47.

[23] Zhang Y-D, Wang J, Wu C-J, Bao M-L, Li H, Wang X-N, et al. An imaging-based approach predicts clinical outcomes in prostate cancer through a novel support vector machine classification. Oncotarget 2016;7:78140–51.

[24] Cosma G, Acampora G, Brown D, Rees RC, Khan M, Pockley AG. Prediction of pathological stage in patients with prostate cancer: a neuro-fuzzy model. PLoS One 2016;11:e0155856.